Low-level jets in the NASA Ames Mars general circulation model

M. M. Joshi, R. M. Haberle, J. R. Barnes,[1] J. R. Murphy,[2] and J. Schaeffer[3]

Space Science Division, NASA Ames Research Center, Moffett Field, California

Abstract. Previous simulations of the Martian atmosphere have shown how topography acts to confine the low-level Hadley cell flow into intense jets on the eastern flanks of Tharsis and Syrtis Major. We now conduct detailed studies of these jets using the NASA Ames Mars general circulation model (MGCM). The structure of the flow is found to be sensitive to local topography as well as large-scale diabatic heating patterns, consistent with terrestrial studies, and MGCM studies carried out with simplified topography. The summer subtropical zonal winds associated with the Hadley circulation also form spatially confined intense jet cores. Diurnal variations in heating affect jet structure in three distinct ways. Global tides interact with the jets, resulting in effects such as the two reinforcing each other at the summer subtropics near midday, leading to high winds and surface stresses at this time. Slope winds act to change the character of the jets during the course of a day, especially at Syrtis Major and the Hellas basin, where slopes are large. Vertical mixing acts to decrease low-level winds during the late afternoon. The sensitivity of the results to atmospheric dust loading is examined. We finally show how a decrease in boundary layer height due to dust loading actually augments mid-afternoon jet strength near the surface. The resulting increase in maximum surface stress indicates that this is a positive feedback to dust lifting.

Introduction

At most times of the year, the time-mean tropical Martian circulation is thought to be dominated by a single cross-equatorial Hadley cell [*Haberle et al.*, 1982]. Viking Lander 1 (VL1) observations of wind are also consistent with this type of circulation [*Murphy et al.*, 1990]. During the solstices, this cell enlarges in amplitude and latitudinal extent, peaking at 6 times the magnitude of its terrestrial counterpart after taking into account the differing atmospheric masses [*Haberle et al.*, 1993b]. The intensity of the Martian Hadley cell results in part from the latitude of maximum upward motion being centered well away from the equator [*Lindzen and Hou*, 1988]. This is because the Martian surface has a relatively low thermal inertia and reacts quickly to seasonal changes in solar heating, whereas on Earth, the oceans inhibit the terrestrial Hadley circulation from undergoing such large seasonal changes. Increasing dust loading in the Martian atmosphere acts to intensify the Hadley cell due to the increased atmospheric heating [*Haberle et al.*, 1993b].

Recently, it has come to light that the lower branch of the Hadley cell is strongly topographically controlled [*Greeley et al.*, 1993]. General circulation model (GCM) simulations employing simplified algorithms of heating and frictional processes showed how low-level cross-equatorial flow took the form of intense jets, akin to the East African Jet on Earth. These jets were interpreted as having the character of western boundary currents (henceforth WBCs)[*Joshi et al.*, 1995]. These jets have now been identified in another GCM of the Martian atmosphere [*Wilson and Hamilton*, 1996].

On Mars, strong westerly winds are present in the summer subtropical regions, arising from constraints of angular momentum. Fluid parcels are accelerated toward the east as they leave the equator in order to conserve the total (fluid+planetary) angular momentum of each parcel [*Haberle et al.*, 1993b; *Hourdin et al.*, 1993]. These latitudes are also coincident with the regions where global dust storms have been seen to start [*Martin and Zurek*, 1993].

Previous Work

In the presence of rotation, and in the absence of any meridional barrier, it can be shown that low-level cross-

---

[1]Also at Department of Atmospheric Sciences, Oregon State University, Corvallis.
[2]Also at San Jose State University Foundation, San Jose, California.
[3]Also at Sterling Software, Inc., Palo Alto, California.

equatorial flow from winter to summer hemispheres takes the form of a parabola, i.e., on an equatorial β plane, the streamlines have the form $x = Ay^2 + By + C$ [*Anderson*, 1976], where x and y are non-dimensionalized cartesian coordinates. Fluid parcels will always cross the equator to the west of the forcing region where they originate. *Anderson* [1976] showed using a quasi-barotropic β plane model that the distance $\Delta\lambda$ between the longitude of heating and the longitude of cross-equatorial flow was dependent on friction, and could be found by solving the equation for the streamlines $x = y_0^4/24K$, where K is the eddy mixing coefficient.

If a meridional boundary intersects the streamlines, this flow is constrained into a narrow jet at the equator. This situation is analogous to western boundary currents in Earth's oceans [*Gill*, 1980, p.512].

Joshi et al.[1995] used a simplified three-dimensional (3-D) model of Mars to show how cross-equatorial flow was topographically controlled in the same manner as the East African jet, which controls the cross-equatorial flow associated with the Asian monsoon [*Hoskins and Rodwell*, 1995]. The most intense flow was on the eastern flank of the Tharsis Plateau at about 45°W, with a rather weaker jet present on the eastern flank of Syrtis Major near 80°E.

Topographically forced slope winds, forced by horizontal density gradients, are common on Mars in the tropics [*Savijärvi and Siili*, 1993]. It was shown that these winds could act to cancel or reinforce the Syrtis WBC at different seasons due to the meridional direction and large amplitude (0.2°) of the topographical slope at this longitude [*Joshi et al.*, 1995].

The model used by Joshi et al. represented diabatic processes by Newtonian relaxation, and surface friction by Raleigh friction in the lowest model level only. It did not take account of the effect of enhanced heating over upland regions. This effect was tested by M. Joshi et al. (Seasonal variations in low-level flow in the NASA Ames Mars GCM, submitted to *Advances in Space Research*, 1996, hereinafter referred to as submitted paper), who ran the Ames Mars GCM (MGCM) under conditions of $L_s = 270$, and $\tau = 0.3$, but with two idealized topography sets. One had a representation of an idealized Gaussian-shaped Tharsis Plateau, and one had an idealized Tharsis and Syrtis Major. Both runs had albedo varying as in the nominal MGCM. The first run displayed some longitudinal variations in time-mean v, but only when Syrtis Major was included did a strong jet form on the eastern flank of the idealized Tharsis. This result is similar to that obtained by *Rodwell and Hoskins* [1995], who found that local topography and distant heating controlled the behavior of the East African jet in their simulations.

We now present more detailed simulations of low-level jets in the NASA Ames MGCM. The horizontal and vertical structure of these flows is discussed, and the effect of longitudinal variations in heating with real topography and albedo examined. The diurnal variations in these jets are examined, and the mechanisms involved discussed. The effect of static dust loading is looked at. We conclude with a discussion of the effects of these jets on dust storm behavior, and the explanation of a possible new positive feedback to dust lifting associated with low-level jets.

The NASA Ames Mars GCM

The NASA Ames MGCM is a grid point model that solves the primitive equations of meteorology on the sphere [e.g., *Andrews et al.*, 1987, p.114]. It employs a modified σ coordinate system in the vertical, where $\sigma = (p - p_T)/(p_S - p_T)$, p_S is the surface pressure, and p_T is the tropopause pressure set to 0.07 mbar. The pertinent differences between this model and the simplified model used by *Joshi et al.* [1995] are the physical parameterizations. The MGCM has a sophisticated scheme for calculating radiative heating and cooling by atmospheric CO_2 and suspended dust, and also represents the seasonal CO_2 condensation flow. Details of these processes are given by *Pollack et al.* [1990].

The planetary boundary layer (hence PBL) is handled in a much more sophisticated manner than the simpler models. The following algorithm is used.

1. For each model column the height of the (convectively) unstable boundary layer is diagnosed from the model. This height can never be lower than the midpoint of the lowest model level, which lies at a height of approximately 250 m above the surface.

2. Heat and momentum are then uniformly mixed within this domain.

3. Surface heat and momentum fluxes are then calculated and assumed to decrease linearly with pressure to the top of the PBL. The algorithm for calculating these fluxes is given by *Pollack et al.* [1990].

This algorithm may seem involved, but it should be noted that it differs from other GCMs in that surface fluxes are mixed within the whole PBL, rather than just added to the lowest model level, making the magnitude of these fluxes independent of vertical model resolution. In order to do this, the height of the PBL must already be known.

At the time of writing, the uniform momentum mixing is being replaced by a more sophisticated algorithm of vertical momentum transfer, based on that used by *Haberle et al.* [1993a].

Time Mean Structure

In order to simplify model run description, we present in Table 1 a summary of the runs analyzed for this study. Runs were done for the two solstice seasons, with dust optical depth fixed at $\tau = 0.3$, and with different topography data sets. Some runs at $L_s = 270$ were performed with higher opacities, as this is the season where great and global dust storms are most often seen to start [*Martin and Zurek*, 1993.]

Table 1. Run Identifier Numbers for Each Model Run

Topography	Opacity τ	$L_s = 90$	$L_s = 270$
Billiard ball	0.0	-	B0
	0.3	-	B2
Flat topography	0.3	F1	F2
Zonally symmetric topography	0.3	Z1	Z2
	1.0	–	Z4
Consortium topography	0.3	T1	T2
	1.0	–	T4
	5.0	–	T6

The Equatorial Jets

Figure 1 shows-time averaged low-latitude winds at the two solstice seasons $L_s = 90$ and $L_s = 270$ (runs T1 and T2, respectively) on the lowest model level, which lies approximately 250 m above the surface. At $L_s = 90$ the flow is concentrated into three tight bands at the equator, east of Tharsis (at 45°W), Syrtis (at 90°E), and south of Elysium (west of 180°E), consistent with earlier simulations [*Wilson and Hamilton*, 1996]. At $L_s = 270$, these jets are broader. In the latter season, the low-level westerly ITCZ (Inter-tropical Convergence Zone) jet is also apparent. Note that in this context ITCZ is used as a short form to denote the Martian summer subtropical latitudes. This jet displays a significant amount of zonal asymmetry. Not only this, but the jet is almost absent at $L_s = 90$.

Longitude-height sections of meridional wind v at the equator are shown in Figure 2. At both seasons, the flow in the equatorial jets is most intense at the lowest model level, with Tharsis jet winds reaching 25 m s^{-1} at $L_s = 90$, and 30 m s^{-1} at $L_s = 270$. These winds are of similar orders of magnitude, even though the Hadley cell is twice as intense at $L_s = 270$ [*Haberle et al.*, 1993b]. Moreover, the Tharsis jet at $L_s = 270$ is less tightly confined in longitude than its $L_s = 90$ counterpart. Indeed, a fourth jet seems to exist on the top of the Tharsis Plateau at 100°W. This jet appears to be a manifestation of an downslope flow on the southeastern flank of Tharsis (see Figure 1.)

Diabatic Heating

M. Joshi (submitted paper, 1996) demonstrated the importance of zonally asymmetric heating on forcing low-level jets by using idealized topography data sets. The effect of full topography and albedo are now considered in detail.

The actual amount of solar radiation absorbed by the ground is broadly proportional to 1-a, where a is the ground albedo. The resulting heating of the atmosphere is inversely proportional to pressure, and is therefore dependent on topography. The value of 1-a can vary between 0.7 and 0.85 in the tropics (or ±10%), while pressure varies between 3 and 6 mbar (or ±50%). This

means that topography should be the more important factor in controlling near surface heating.

The forcing of the low-level flow was examined by looking at the vertical convergence of the sensible heat flux from ground to atmosphere, and is shown in Figure 3. The heating is far more zonally asymmetric during $L_s = 90$ than during $L_s = 270$. In both seasons, the location of the most intense heating is the Tharsis Plateau, and so a large component of the flow crosses the equator approximately 60°W of this region, but east of the Syrtis region. The phenomenon of western intensification is therefore not so pronounced in this case. This broadening of the Syrtis flow at both solstice seasons was also seen in the intermediate model of *Joshi et al.* [1995], which accounted for the enhanced heating over tropical upland regions.

Northern summer exhibits greater heating at 0°E to 40°E compared to other longitudes due to the presence of Syrtis Major. This relative extra heating does not exist in the southern hemisphere. This results in greater cross-equatorial flow to the west of the heating, and a relatively more intense Tharsis jet, given the less intense mean Hadley cell strength at this time.

The jet over Tharsis during $L_s = 270$ at 100°W (see Figure 2) cannot be explained by zonal asymmetries in heating. However, slope winds may be the cause of this phenomenon. Figure 1 shows intense downslope winds at this season near 100°W over the steep slopes of the Tharsis plateau. These winds do not form a coherent equator-crossing jet as at 45°W, but exist in the summer subtropics. The most likely explanation for this jet is therefore that it is the residual effect of a slope wind circulation.

The longitudinal confinement of heating implies a similar asymmetry in the vertical velocity ω. This is shown in Figure 4. The 4-mbar surface is chosen, as this is where $\overline{\omega}$ is at its greatest in the subtropics in both seasons [e.g., *Haberle et al.* 1993b, Figure 4a]. At $L_s = 90$, there are two locations of ITCZ uplift at 60°W and 60°E. These longitudes are coincident with the strong northward flow at low levels seen in Figure 2. At $L_s = 270$, the longitudinal extent of high values of ITCZ ω is greater than in the other season, again coincident with the broader cross-equatorial flow seen at this time (see Figure 2).
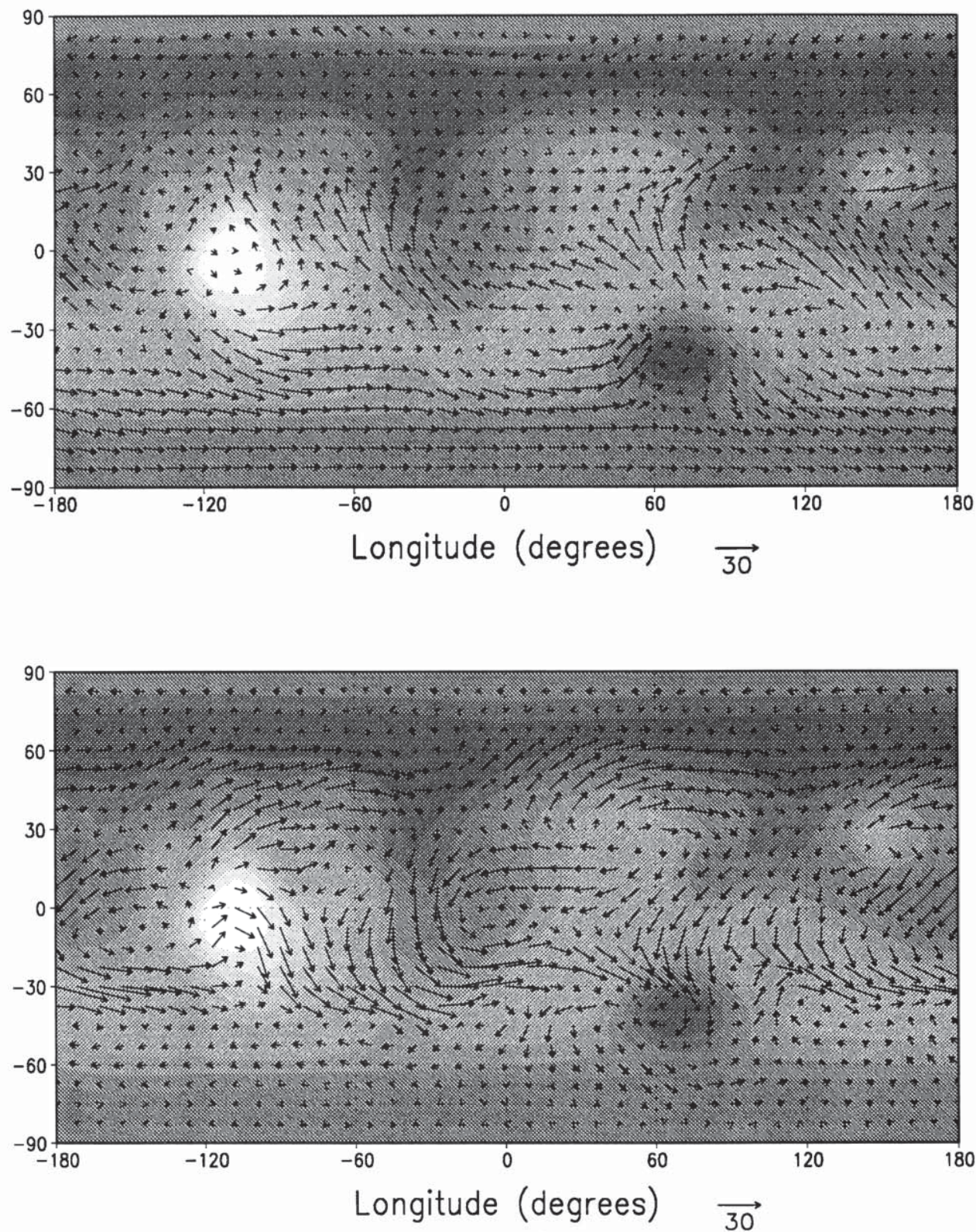
Figure 1. Twenty-sol time-mean wind vectors (m s^{-1}) on the lowest model σ level superimposed on shaded topography. (Top) $L_s = 90$ (run T1). (Bottom) $L_s = 270$ (run T2). The topography shading is in 1-km intervals from grey (lowest) to white (highest). Note the convention of using longitudes increasing from 0°W to 180°W, rather than some maps which use longitudes decreasing westward from 0°E/360°E to 180°E.
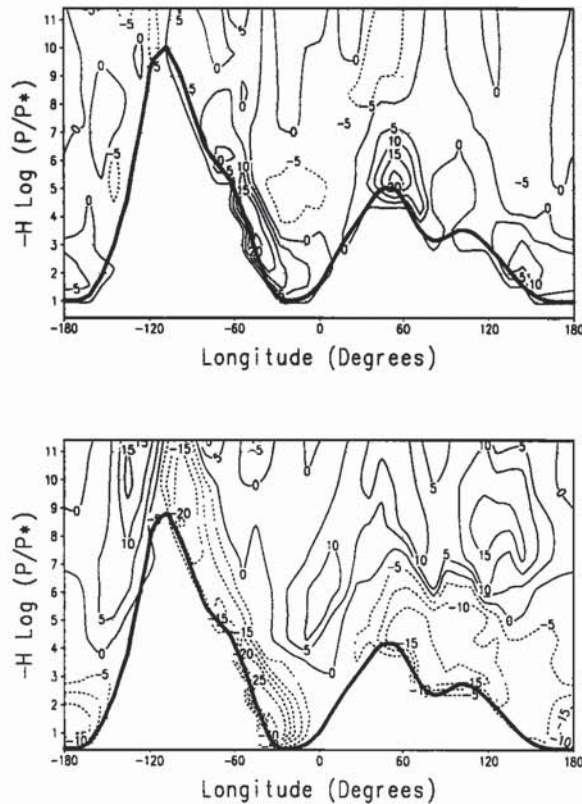
Figure 2. Longitude-log(pressure) section of time-mean v at the equator at (top) L_s=90 (run T1) and (bottom) L_s =270 (run T2) (m s^{-1}). The thick contour shows the surface (difference between the two plots due to seasonal pressure changes). Note that since u and v are not explicitly calculated at the equator in the MGCM, this is the result of an interpolation between the two adjacent latitudes (3.75°N and 3.75°S in this case).

The zonal asymmetry in heating and ω results in asymmetries in the cross-equatorial mass flow. Trying to analyze the distance between the heating longitude and the cross-equatorial flow longitude using the analysis of *Anderson* [1976] is difficult, as accurate values of K, the eddy mixing coefficient, cannot be derived from the uniform momentum mixing. However, by simply looking at wind vectors in Figure 1, it can be seen that the longitude of most intense meridional flow is 30-60°W of the forcing longitude, depending on how far away the forcing area is from the equator.

The lower branch of the Hadley cell is contained within the lowest three model levels (σ=0.98, 0.90, and 0.80) at both seasons. The total mass flow in these levels (normalized by the total flow at each level) is shown in Figure 5. The Tharsis jet (defined as being from 18°W to 60°W) carries about 27% of the total cross-equatorial mass flow at L_s =270, whereas its counterpart at L_s = 90 carries about 35%. This is again an indication of the relatively more intense Tharsis jet at L_s = 90.

The importance of surface albedo compared to topography was tested by redoing run T1, but with a constant albedo (denoted run T1A). The sensible heating in this case is shown in Figure 6. The spatial pattern is very similar to run T1. The difference field T1A-T1 is also shown in Figure 6 (bottom). Run 1A exhibits greater heating in the northern hemisphere due to its lower albedo. Only at 60°E, where the nominal albedo is low [e.g., *Christensen and Moore*, 1992, Figure 7] is the heating lower in run T1A. The differences are $O(20\%)$ of the actual heating, consistent with the scaling argument given above.

The cross-equatorial mass flow in runs T1 and T1A was then compared with run Z1, which contained zonally symmetric topography, but had nominal albedo. The results are shown in Figure 5. Run T1A has no zonal variations in albedo, and yet the jet patterns are almost the same as in run T1. Run Z1 does exhibit zonal variations in mass flow, although these are not very large. The Tharsis jet is 10-20% weaker in run T1A. This is another indication that topography is the controlling factor in determining cross-equatorial jet strength. The sensitivity study T1A was only carried out for $L_s = 90$, as the northern subtropical albedo field is far more zonally asymmetric than the south [see
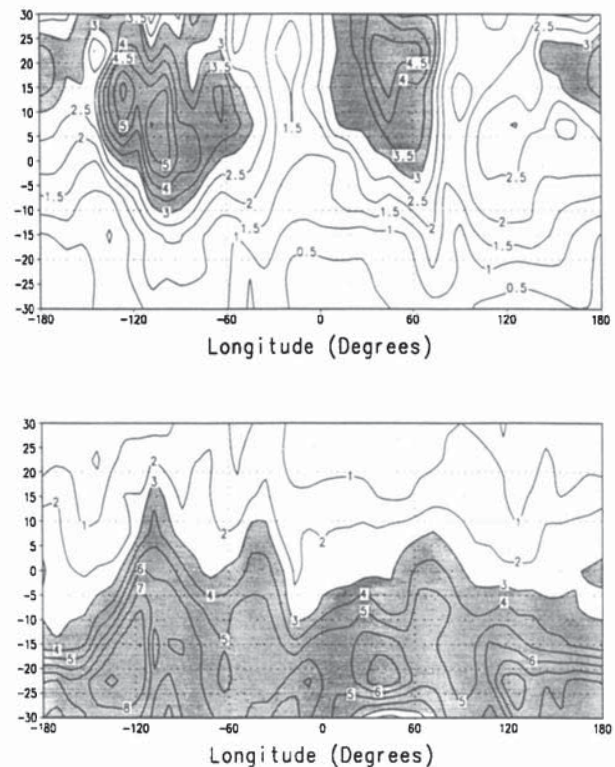

Figure 3. Heating due to sensible heat flux convergence in the MGCM at (top) L_s=90 (run T1) and (bottom) L_s =270 (run T2) (K sol^{-1}). The plots are averages from the model bottom to a height of 6 km, and values above 3 K sol^{-1} are shaded.
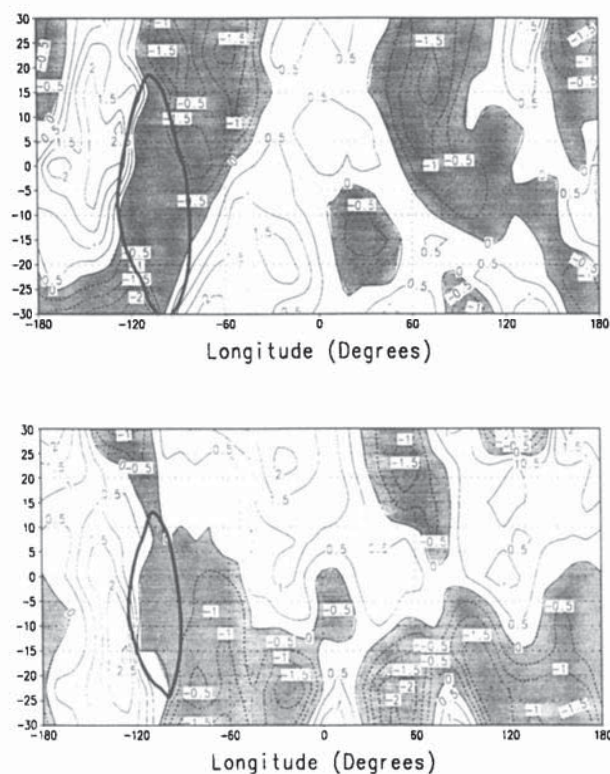
Figure 4. Time-mean ω on the 4-mbar surface in units of mbar sol^{-1} at (top) $L_s = 90$ and (bottom) $L_s = 270$. The shaded areas indicate negative (upward) values of ω. The thick contour encloses the area where this pressure surface lies below the ground (note again this is different for the two seasons).
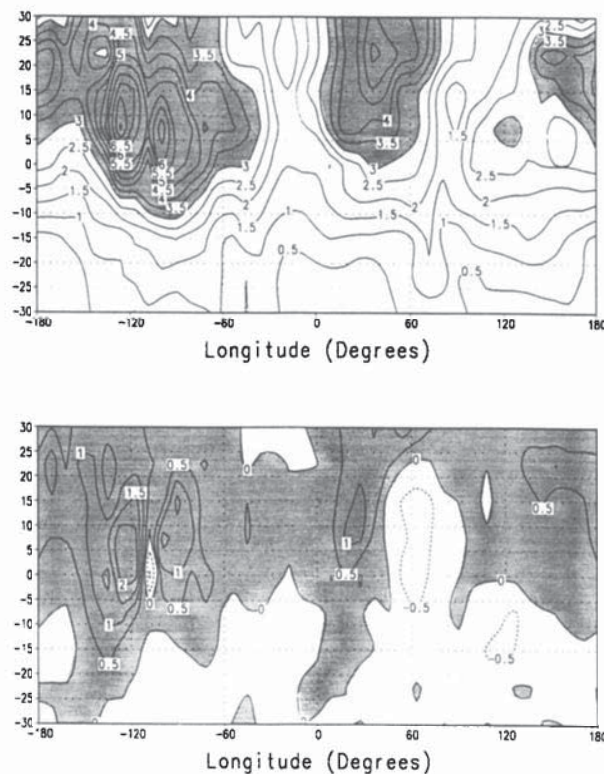
Figure 6. As in Figure 3 but for run (top) T1A (constant albedo) and (bottom) the difference field T1A-T1.

Christensen and Moore, 1992, Figure 7]. However, the cross-equatorial flow in run Z2 was analyzed in order to compare it with run T2. This is also shown in Figure 5. It can be seen that this is almost zonally symmetric.

Sensitivity to Topography Data Sets

Since the flows are sensitive to topography, the effect of using different data sets was checked. Run T2 was repeated, except the digital terrain model (DTM) [*Wu*, 1978] was used. At $L_s = 90$ the mean meridional circulation using the DTM was 10% weaker than with using the consortium set: at $L_s = 270$, the strengths were equal to within 1%. This is because the major differences between the data sets occur in the northern hemisphere, so heating centered there (at $L_s = 90$) will display the greater asymmetry. There were slight differences in jet strength, but the broad patterns remained the same.

Run T2 was repeated using a newer topographic data set [*Smith and Zuber*, 1996]. This run displayed a cross-equatorial jet at Tharsis shifted westward from 45°W
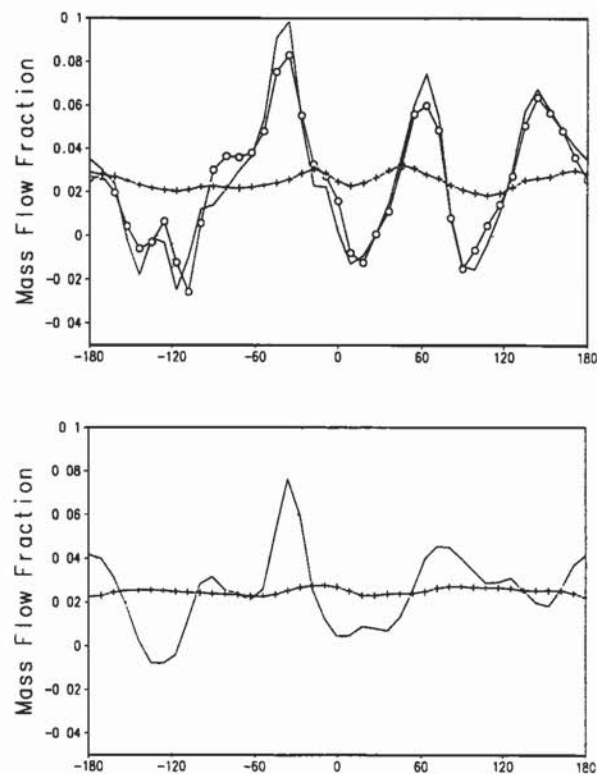
Figure 5. The fraction of the total cross-equatorial mass flow in the lowest three model levels carried at each longitude at the equator in run T1 (top, unmarked curve), run Z1 (top, crosses), run T1A (top, open circles), run T2 (bottom, unmarked curve) and run Z2 (bottom, crosses) (units are kg s^{-1}).
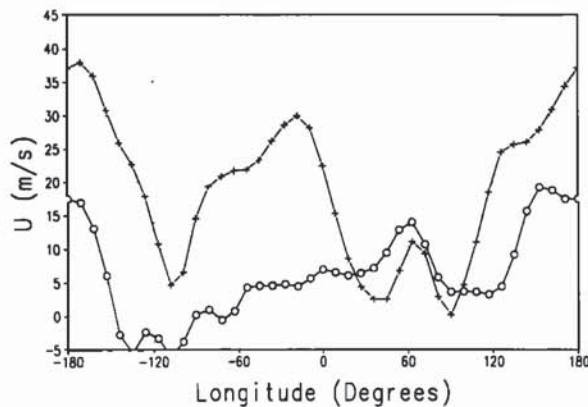
Figure 7. Zonal wind u in the lowest model level at L_s = 90 (run T1)(open circles) at 22°N and L_s = 270 (run T2)(crosses) at 30°S (m s^{-1}). In each case the latitude is chosen where each jet is at its most intense [*Haberle et al.* 1993b].
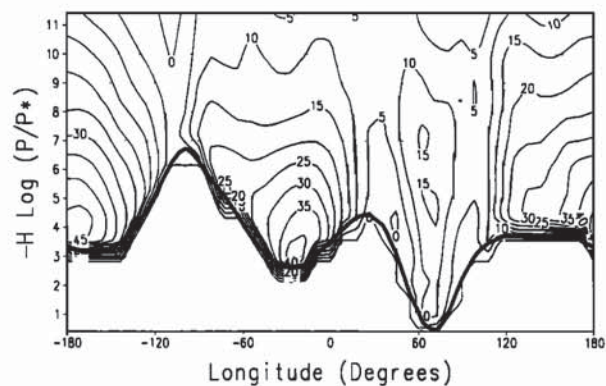

Figure 8. Longitude-log(pressure) section of time-mean u at 30°S during L_s = 270 (run T2) (m s^{-1}). The thick contour shows the surface.

in the nominal simulations to 70°W. The location and strength of the Syrtis jet was almost unchanged in the new run. Observational evidence for WBCs in the form of dust streaks and locations of preferred dust lifting at the equator indicate that the Tharsis jet lies at about 40-50°W [*Joshi et al.*, 1995]. The inconsistency could be an indication of a phenomenon not represented by the GCM causing actual dust lifting at 40-50°W, but this then is inconsistent with the fact that relatively few dust events have been observed at the equator between 70°W and 90°W, which is where the MGCM with the new data set predicts very high winds and stresses.

An accurate Martian topographic data set should be obtained in the near future by the Mars Observer laser altimeter (MOLA) instrument aboard Mars Global Surveyor (MGS). The precise structure and location of low level jets cannot be fully known until then.

The Subtropical Jets

The westerly zonal winds present in the subtropics are evident in Figure 7. At both seasons the jets display a large degree of longitudinal asymmetry. At L_s = 270, the strongest winds occur at about 30°W and near 180°E, just to the east of the longitudes of intense cross-equatorial flow. This is because angular momentum is not conserved in the low-level flows, and so u in the summer subtropics is dependent on the cross-equatorial v. The size of these subtropical jet cores is related to the longitudinal extent of the cross-equatorial flow, e.g., the jet core at 30°W is relatively narrow, whereas the jet core at 180°W has more extent in longitude.

Topographic effects play a large role in changing local jet strength in a number of ways. Intense slope winds associated with the Hellas basin interact with the jet at between 40° and 80°E at L_s = 270 (see below). In fact, this region actually exhibits time-mean easterlies near 80°E, 30°S. As shown in Figure 1, the region between 120°E and 150°W is very flat, and mountain

torques will have relatively small magnitudes here, allowing winds to build up to very high speeds in this region. This was noted in an MGCM simulation with flat topography, where the ITCZ jet reached speeds twice as high as when topography was included [*Haberle et al.*, 1993b].

The vertical structure of the southern summer jet is shown in Figure 8. As before, the peaks at 30°W and 150°E can be made out. Unlike the meridional flow at the equator, the zonal jet peaks in strength further away from the surface, at a height of about 1 km. Its vertical scale is also much greater, reaching above a scale height.

Diurnal Variations

The effects of global tides, vertical mixing in the PBL, and slope winds are now considered in turn. Although it is not expected that a linear superposition of each of these effects would exactly predict MGCM wind strength, looking at each phenomenon individually can help to clarify its effect on the MGCM circulation.
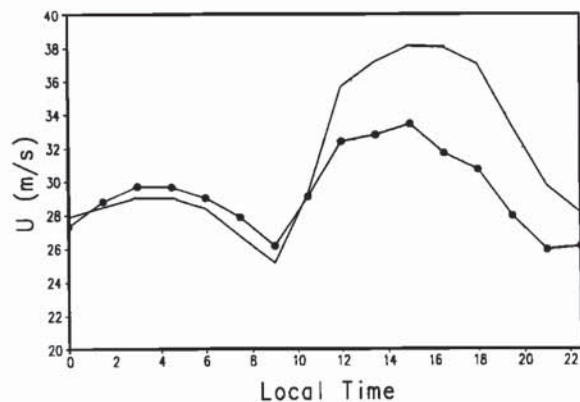

Figure 9. Variation of zonal wind u (m s^{-1}) with local time at 30°S in run F2 (unmarked curve) and run Z2 (dots).

Tidal Interaction

Global-scale tides will tend to reinforce or cancel the
low-level flows at certain times of day, depending on
the flow direction and the tidal strength. In order to
assess this affect without the complicating effect of to-
pography, two runs with flat topography were carried
out, denoted F1 and F2 (see Table 1). Albedo and ther-
mal inertia in these runs were as in the nominal cases.
Diurnal wind composites were constructed from 10 sols
(1 sol = 1 Martian day = 24.6 hours) of model output
by the following method: given a grid point sampled n
times every sol, n records were made by averaging data
from time indices $x, x+n, x+2n, ..., x+9n$. This had
the effect of removing all frequencies below 1 sol ex-
cept the time-mean. An averaging period of 10 sols was
chosen, as there was no significant variation below this
frequency in the tropics at low levels (although there is
a great deal at high levels [*Barnes et al.*, 1993]).

Figure 9 shows the diurnal variation of u in run F2
(solid line with no symbols). In the summer subtrop-
ics, u reaches its maximum values during late afternoon
and early morning. The maximum during the afternoon
occurs despite the effect of vertical mixing acting to de-
celerate the jet at low levels. However, it is consistent
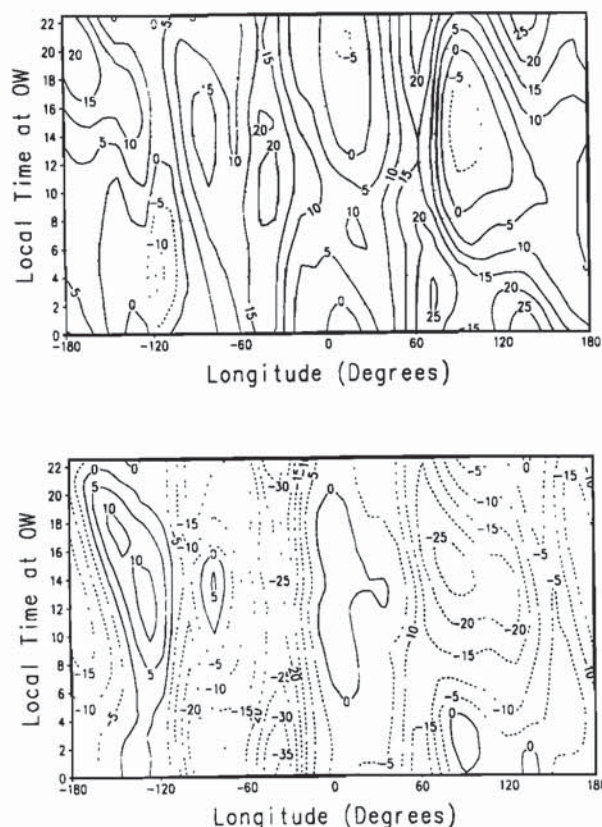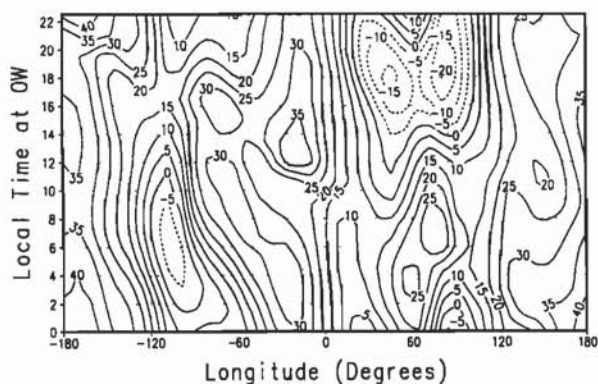
Figure 11. Hovmuller plot of variation of u (m s^{-1})
with local time in run T2 at 30°S in the lowest model
level.

with the reinforcement of the low-level jet by the tides.
Leovy and Zurek [1979] showed that at the VL1 site (at
22°N), semidiurnal zonal wind maxima occurred at this
local time. The same should hold true for the south-
ern hemisphere tropics as well (with relatively low dust
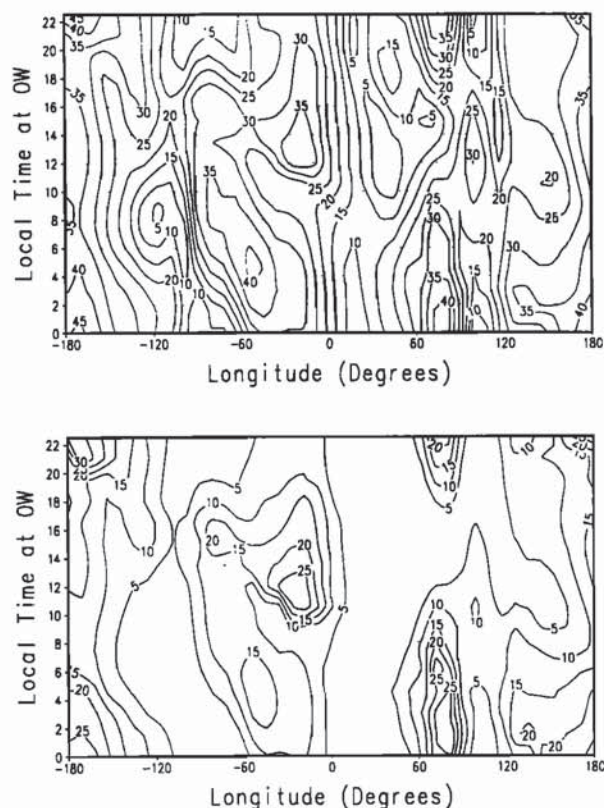loading).

Effect of Topography

The effect of the zonal topographical slope was tested
by comparing the diurnal variation of u and v in runs
F1 and F2 with winds in two runs (Z1 and Z2; see Table
1), which incorporated the zonally averaged component
of the Consortium data set.

The variation of u at 30°S in run Z2 is shown in
the solid line with dots in Figure 9. The zonal wind u
still exhibited a maximum during the afternoon, as in
runs F1 and F2, although it occurred about 2 hours ear-
lier, and the maximum value reached was much smaller.
This was because the surface pressure at 30°S is far
lower in run Z2 than in F2, and the former therefore
exhibits greater heating and a deeper PBL. The maxi-
mum height reached by the PBL is 6.5 km in run Z2,
as opposed to 8.5 km in run F2. The main differences
occur in the afternoon, which is where the difference is
seen in between the two curves in Figure 9.

The diurnal variation of v at the equator in runs T1
and T2 is shown in Figure 10. Three distinct regimes
are evident at both seasons. Between 60°W and 20°W,
the intense WBC prevails, which displays intense merid-
ional winds throughout the day, although there is some
diurnal variation in its strength. Between 20°W and
40°E, flow is weak at all times of the day. Elsewhere,
large diurnal variations occur due to the large merid-
ional slopes present.

The temporal variation of the ITCZ jet in run T2 is
shown in Figure 11. The two westerly jet cores are ap-
parent at 0-40°W and 120-210°E, coincident with the
longitudes of maximum southward flow at the equator.
In these jet cores the highest winds occur just after
midday, which is slightly earlier than the flat simula-

Figure 10. Hovmuller plot of variation of v with local
time at (top) $L_s = 90$ (run T1) and (bottom) $L_s = 270$
(run T2) (m s^{-1}) at the equator in the lowest model
level.

Figure 12. Hovmuller plot of variation of (top) $|u|$ (m s^{-1}) and (bottom) surface stress τ (mPa) with local time in run T2 at 30°S in the lowest model level.

tions carried out above. This can be explained by the fact that, as in run Z2, the upslope (southward) wind is turned by the Coriolis force toward an eastward direction just after midday [*Savijärvi and Siili*, 1993] and reinforces the ITCZ jet.

The fact that at 30°S u maximizes during the afternoon is important when considering dust lifting, which is dependent on surface stress, which in turn, is a function of wind speed as well as static stability. During the day, when the atmosphere is unstable, high winds will lead to high stresses. Conversely, during the night, even though winds are high, stresses are low due to the high static stabilities. This is apparent in Figure 12, which shows diurnal composites of low-level wind speed and surface stress τ. Although there are high winds in the morning at 50°W, this is not reflected in the surface stress.

The wind speed maxima during the day (e.g., at midday at 20°W) give rise to large stresses in excess of 30 mPa, which is in the range required to lift dust by saltation [*Greeley and Iversen*, 1985], so the maximum stresses observed in the MGCM at these latitudes should be able to lift dust from the Martian surface. These longitudes are in fact coincident with locations where global dust storms have been seen to originate [*Martin and Zurek*, 1993].

The flow over Syrtis experiences intense diurnal modulation, with the largest variation occurring at 90°E, where the meridional slope is largest (see Figure 1). Here v varies by up to 25 m s^{-1} over the course of a day. The phase of the slope wind is such that the maximum upslope (negative) v occurs in late afternoon. This upslope wind tends to reinforce the mean flow at $L_s = 270$ and cancel it at $L_s = 90$, as predicted by *Joshi et al.* [1995]. Indeed, as with the global tide reinforcing the ITCZ jet during late afternoon, the highest winds over Syrtis are found at about 1800 hours at $L_s = 270$.

Very large diurnal variations also occur at 120°W and 60°E, where slope winds associated with the Tharsis and Hellas regions, respectively, disrupt the westerly flow. The largest variation is about 50 m s^{-1} over a day, and occurs over the northeast flank of Hellas.

Effect of Vertical Momentum Transport

In the equatorial jets, winds peak in the lowest model level and die out ≈ 5 km above the surface. In this case, momentum mixing reduces jet strength in the lowest model level. However, in the ITCZ jet, winds peak at about 1 km above the ground (see Figure 8). This means that vertical momentum mixing will have two distinct effects on winds in the lowest model level. When the top of the PBL is less than 2 km high (before noon), momentum is mixed between the lowest two model levels only, which has the effect of increasing winds in the lowest model level. In the afternoon the PBL reaches heights in excess of this, and momentum is mixed within the lowest 10 km of the atmosphere, lowering winds near the surface. A schematic of this process is shown in Figure 13.

It is generally assumed that the unstable PBL is well mixed [e.g., *Savijärvi and Siili*, 1993], and vertical eddy mixing coefficients are $O(10^3)$ m^2 s^{-1}. However, the instantaneous mixing present in the MGCM leads to inferred values of nearly 10^4 m^2 s^{-1} when the PBL reaches heights of 10 km and is therefore probably too intense. While inclusion of the new PBL scheme should alleviate this problem, we note that the effects of vertical mixing
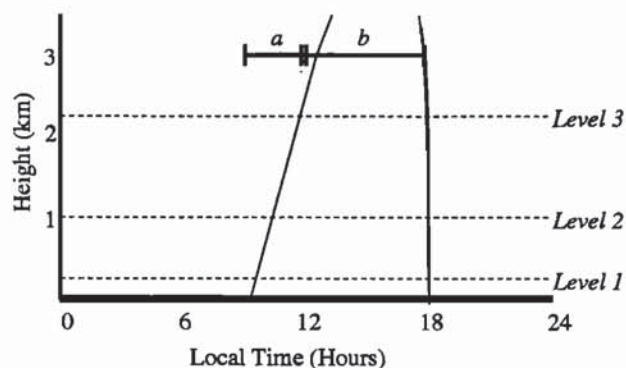
Figure 13. Schematic showing the behavior of the PBL during the day. During regime a the PBL encompasses only the lowest two model levels; during regime b the PBL reaches far above this height.
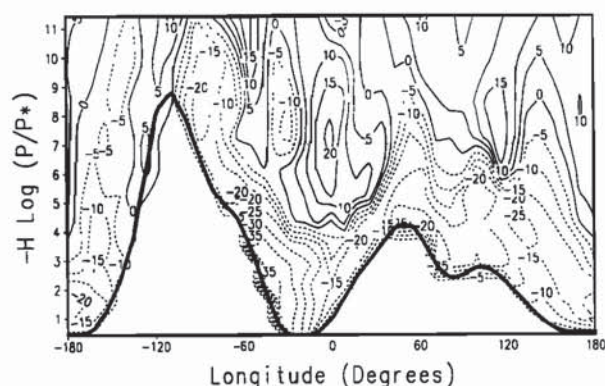
Figure 14. Longitude-log(pressure) section of time-mean v (m s^{-1}) at the equator in run T6. Negative contours are shaded.

on surface winds and stresses shown above should still stand, at least qualitatively.

The Effect of Dust

Static Dust Loading in the MGCM

Dust acts to intensify the Hadley cell and therefore the low-level jets associated with it [*Haberle et al.*, 1993b]. However, dust also affects the diurnal circulations that interact with these jets, so the total time-averaged dusty wind fields will not be simple linear multiplications of those with low dust loading. These effects were examined by analyzing a MGCM run carried out with opacity τ set to 1.0 and 5.0. These runs were denoted T4 and T6 (see Table 1).

Interestingly enough, while run T6 exhibits a mean meridional circulation that is about 1.5 times as strong as T2, peak winds in the lowest model level at 45°W do not increase by this amount. Between runs T2 and T6 the peak v at 45°W increases from about 35 m s^{-1} to 40 m s^{-1}. Figure 14 shows that the meridional flow is spread throughout a greater horizontal domain, and so a smaller fraction of it is carried through the Tharsis and Syrtis jets. This is because when the dust optical depth equals 5, half the incoming solar radiation is absorbed in the atmosphere and does not reach the ground [see *Pollack et al.*1990, Figure 1]. The effect of zonal asymmetries in surface heating is diminished, and the effect of zonally uniform dust heating becomes more important. The cross-equatorial flow responds to this by becoming more zonally uniform.

As dust loading increases, there is a steady westerly increase in u, with time-averaged values of u peaking above 40 m s^{-1} in run T6. The variation of u in run T6 with local time is shown in Figure 15 and clearly shows the zonal component of the Hellas slope winds strongly varying with local time. The afternoon maximum of the westerly component of the flow can also be seen. When compared with Figure 11, it can be seen that the time

of maximum u has advanced from midday to nearer 1600 hours, consistent with the effect of the stronger semidiurnal tide in this run. However, it must be noted that the PBL top has also dropped from a maximum height of 15 km in T2 to 3 km in T6, indicating that the effect of vertical mixing has also lessened. It would appear that both effects are present in the dusty PBL.

Low-Level Jets and Dust Storms

As shown in Figure 12, stresses >30 mPa occur at 30°S at 0-30°W, and around 180°W, in the ITCZ jet cores. The fact that these stresses occur during the daytime has implications for the vertical transport of dust. Turbulent eddies will act to mix dust efficiently in the vertical up to heights of 10-15 km during the daytime. Dust raised from the surface at this time will therefore be more likely to be lifted high into the atmosphere than dust raised during the night, where turbulence is mechanically generated, and dies out less than 1 km above the ground even in the presence of high winds. Not only that, but since this is the latitude of the ascending branch of the Hadley cell, dust lifted here can be transported efficiently throughout the Martian atmosphere [*Murphy et al.*, 1995].

Previous work has shown how the presence of dust lessens turbulent mixing in the PBL and shuts off dust transport through it [*Leovy et al.*, 1973]. We now show that dust lifting may be actually increased because of increased atmospheric heating alone. The reason is that vertical mixing acts to lower wind strength during the afternoon when the PBL is about 10 km high (see Figure 13). In the presence of a low-level jet, winds actually peak near the surface and then decrease with height (e.g., Figure 8). Lowering PBL height therefore results in less momentum being lost from near the surface, resulting in a stronger jet there, and hence higher surface stresses. The actual change in surface stress in this idealized case will therefore be determined by the competition between higher winds and higher static stabilities.

Analyzing this feedback in a GCM is difficult, as the presence of dust alters almost all the dynamical pro-
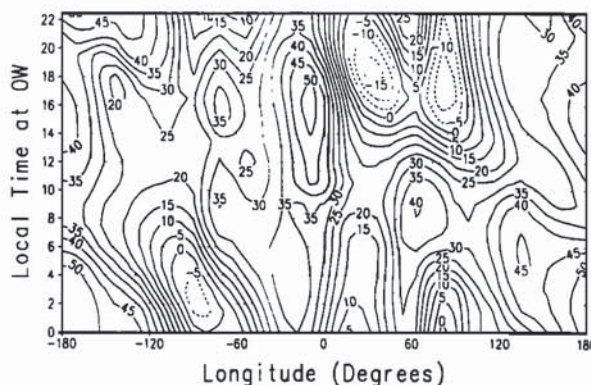
Figure 15. As in Figure 11 but for run T6.
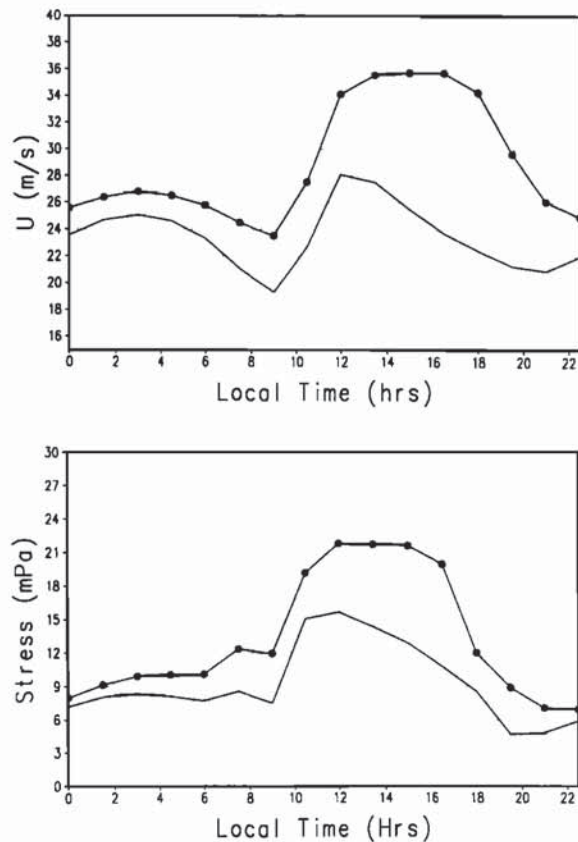
Figure 16. Plots of (top) zonal wind u (m s^{-1}) and (bottom) surface stress (mPa) in runs B0 (unmarked curve) and B2 (dots) at 0°W, 30°S.

cesses present. In order to simplify the analysis, two runs were carried out denoted B0 and B2. In these runs, topography was flat, and albedo and thermal inertia were held spatially constant at 251.9 and 0.22, respectively (apart from the polar caps, where they had their nominal values). The dust optical depths were 0 and 0.3, respectively. Increasing dust optical depth from 0 to 0.3 changed Hadley cell intensity by less than 10% in these runs. This was not reflected in u at 30°S, however. Figure 16 shows u at 0°W, 30°S over the course of a sol. In these runs, u differed by 2 m s^{-1} during the night, but by over 10 m s^{-1} in the afternoon. This increase is reflected in the surface stress, also shown in Figure 16 (bottom). Stresses in run B2 were almost identical to B0 at night, but were almost double B0 during the day. This shows that increasing daytime wind speeds at 250 m from run B0 to B2 acts to increase surface stress, despite the effect of higher static stabilities in the latter case.

One caveat to this feedback is that decreasing PBL height means that dust lifted off the surface will not be mixed as high into the atmosphere, and so has a higher probability of resettling on the ground. This latter negative feedback has been well documented by, e.g., *Leovy et al.* [1973]. However, vertical velocities in

the rising branch of the Hadley cell are at their maximum at about 2-5 km above the surface [*Haberle et al.*, 1993b] at $L_s = 270$. Therefore as long as the top of the PBL is above this height, the positive feedback should dominate, as dust can still be carried out of the PBL by the mean circulation. If the PBL height dips below 2 km, the negative feedback should become important. MGCM simulations show that this happens at $\tau \geq 2.5$ at 30°S, suggesting that below $\tau \equiv 2$ the effect of dust on static stability is a positive feedback to dust raising, while above $\tau = 2.5$ it is a negative feedback.

To sum up, dust lifted into the atmosphere by the ITCZ jet cores at 30°S heats the atmosphere and lowers the maximum height reached by the PBL during the day, thus intensifying these jets even more. It is therefore a positive feedback on the lifting of dust from the surface. The effect of this feedback is only canceled out when the PBL collapses to very low levels at optical depths of unity or so, and vertical transport of dust is significantly impeded to the free atmosphere. More work, using transport models having ensembles of different dust particles such as that used by *Murphy et al.* [1995], is needed to verify this theory.

As shown in Figure 10, winds in the Tharsis jet in run T2 peak during the night, whereas they peak in run T1 during the day, when the PBL is very active. This suggests that even though the time-averaged jet strength is stronger at $L_s = 270$, any dust raised at $L_s = 90$ is most likely to be lifted during the day and can therefore be transported easily through the PBL into the free atmosphere. The Tharsis jet may therefore have as much dust-transporting capability at $L_s = 90$ as it does at $L_s = 270$.

Conclusion

In this paper we have discussed tropical low-level jets that arise in simulations of the Martian climate using the NASA Ames MGCM. Diurnal variations in these jets are caused by interactions between the mean flow and slope winds and thermal tides. Turbulent mixing within the PBL during the day also affects wind strength. The thermal tides act to reinforce the subtropical westerly jet cores during the day, leading to the highest winds actually occurring during the afternoon. This has important implications for dust lifting and transport, since the summer subtropics at $L_s = 270$ are a region where dust storms have been historically seen to originate [*Martin and Zurek*, 1993].

Zonal variations in albedo and thermal inertia play a secondary role in modulating the low-level flow. The topography is most important. Low-level jet behavior is found to be dependent on the dust content of the atmosphere, primarily through its effect on the Hadley circulation, but also through other effects such as the dust-induced changes in the diurnal modulation of the flow.

A potentially important positive feedback between dust loading and the strength of low-level jets has been identified. This mechanism operates by lowering the maximum height that the PBL can reach during the day during dusty periods. Consequently, winds in the low-level jets are mixed to a lesser degree, which has the effect of amplifying winds and surface stresses in the lowest model level.

To conclude, we have shown that tropical low-level jets form an important component of the Martian circulation, and characterizing them is crucial to understanding the time-mean state of the Martian tropics, especially at the solstices. They most probably play a very important role in all phases of major Martian dust storms and therefore in the long-term climate of Mars. Future work will aim to quantify the effect of low-level jets on the transport of tracers such as dust and water. Examining the behavior of the jets in the Martian surface layer, which will aid in confirming their existence from Lander measurements, is also ongoing. Transient variations associated with baroclinic, barotropic, and inertial instabilities will be investigated in detail in the MGCM.

Finally, future observations such as from Mars Global Surveyor are of course necessary in order to shed more light on this phenomenon. Useful data in this regard include images of dust streaks and clouds from the camera and high-resolution temperature data from the radio-occultation instrument [*Hinson and Jenkins*, 1995]. Further into the future, meteorological data gained from lander networks and balloons will constrain and verify MGCM behavior and help us to better understand these jets.

References

Anderson, D. L. T., The low-level jet as a western boundary current, *Mon. Weather Rev.*, *104*, 907-921, 1976.

Andrews, D. G., J. R. Holton and C. B. Leovy, *Middle Atmospheric Dynamics*, Academic, San Diego, Calif., 1987.

Barnes, J. R., J. B. Pollack, R. M. Haberle, C. B. Leovy, R. W. Zurek, H. Lee, and J. Schaeffer, Mars atmospheric dynamics as simulated by the NASA Ames general circulation model, 2, Transient baroclinic eddies, *J. Geophys. Res.*, *98*, 3125-3148, 1993.

Christensen, P. R., and H. J. Moore, The Martian surface layer, in *Mars*, edited by H. Keiffer et al., chap. 22, Univ. of Ariz. Press, Tucson, 1992.

Gill, A. E., *Atmosphere-Ocean Dynamics*, pp. 511-512, Academic, San Diego, Calif., 1980.

Greeley, R., and J. D. Iversen, *Wind as a Geological Process on Earth, Mars, Venus and Titan*, 333 pp., Cambridge Univ. Press, New York, 1985.

Greeley, R., A. Skypeck, and J. B. Pollack, Martian aeolian features and deposits: Comparisons with general circulation models, *J. Geophys. Res.*, *98*, 3183-3196, 1993.

Haberle, R. M., C. B. Pollack, and J. B. Pollack, Some effects of global dust storms on the atmospheric circulation of Mars, *Icarus*, *50*, 322-367, 1982.

Haberle, R. M., H. C. Houben, R. Hertenstein, and T. Herdtle, A boundary-layer model for Mars - Comparison with Viking lander and entry data, *J. Atmos. Sci.*, *50*, 1544-1559, 1993a.

Haberle, R. M., J. B. Pollack, J. R. Barnes, R. W. Zurek, C. B. Leovy, J. R. Murphy, H. Lee, and J. Schaeffer, Mars atmospheric dynamics as simulated by the NASA Ames general circulation model, I, The zonal mean circulation, *J. Geophys. Res.*, *98*, 3093-3124, 1993b.

Hinson, D., and T. Jenkins, Magellan radio occultation measurements of atmospheric waves on Venus, *Icarus*, *104*, 310-327, 1995.

Hoskins, B. J., and M. J. Rodwell, A model of the Asian summer monsoon, I, The global scale, *J. Atmos. Sci.*, *52*, 1329-1340, 1995.

Hourdin, F., P. Le Van, F. Forget, and O. Talagrand, Meteorological variability and the annual surface pressure cycle on Mars, *J. Atmos. Sci.*, *50*, 3625-3640, 1993.

Joshi, M. M., S. R. Lewis, P. L. Read, and D. C. Catling, Western boundary currents in the Martian atmosphere: Numerical simulations and observational evidence, *J. Geophys. Res.*, *100*, 5485-5500, 1995.

Leovy, C. B., R. W. Zurek, and J. B. Pollack, Mechanisms for Martian dust storms, *J. Atmos. Sci.*, *30*, 749-762, 1973.

Leovy, C. B., and R. W. Zurek, Thermal tides and Martian dust storms: Direct evidence for coupling, *J. Geophys. Res.*, *84*, 2956-2968, 1979.

Lindzen, R. S., and A. Y. Hou, Hadley circulations for zonally-averaged heating centered off the equator, *J. Atmos. Sci.*, *45*, 2416-2427, 1988.

Martin, L. J., and R. W. Zurek, An analysis of the history of dust storm activity on Mars, *J. Geophys. Res.*, *98*, 3221-3246, 1993.

Murphy, J. R., C. B. Leovy, and J. E. Tillman, Observations of surface winds in the Martian subtropics, *J. Geophys. Res.*, *95*, 14,555-14,576, 1990.

Murphy, J. R., J. B. Pollack, R. M. Haberle, C. B. Leovy, O. B. Toon, and J. Schaeffer, Three-dimensional numerical simulations of Martian global dust storms, *J. Geophys. Res.*, *100*, 26,357-26,376, 1995.

Pollack, J. B., R. M. Haberle, J. Schaeffer, and H. Lee, Simulation of the general circulation of the Martian

atmosphere, 1, Polar processes, *J. Geophys. Res.*, *95*, 1447-1473, 1990.

Rodwell, M. J., and B. J. Hoskins, A model of the Asian summer monsoon, II, Cross-equatorial flow and PV behaviour, *J. Atmos. Sci.*, *52*, 1341-1356, 1995.

Savijärvi, H., and T. Siili, The Martian slope winds and the nocturnal PBL jet, *J. Atmos. Sci.*, *50*, 77-88, 1993.

Smith, D. E. and M. T. Zuber, The shape of Mars and the topographic signature of the hemispheric dichotomy, *Science*, *217*, 184-188, 1996.

Wilson, R. J., and K. Hamilton, Comprehensive model simulation of thermal tides in the Martian atmosphere, *J. Atmos. Sci.*, *53*, 1290-1326, 1996.

Wu, S. S. C., Mars synthetic topographic mapping, *Icarus*, *33*, 417-440, 1978.

J. R. Barnes, Department of Atmospheric Sciences, Oregon State University, Corvallis, OR 97331.

R. M. Haberle, M. M. Joshi, J. R. Murphy, and J. Schaeffer, Space Sciences Division, MS 245-3, NASA-Ames Research Center, Moffett Field, CA 94035-1000. (email: joshi@humbabe.arc.nasa.gov)